Journal of Applied Polymer Science

Calorimetric Study of Nanocomposites of Multiwalled Carbon Nanotubes and Isotactic Polypropylene Polymer

Parvathalu Kalakonda,[1] Germano S. Iannacchione,[1] Michael Daly,[2] Georgi Y Georgiev,[2] Y. Cabrera,[3] R. Judith,[3] Peggy Cebe[3]

[1]Department of Physics, Worcester Polytechnic Institute, Worcester, Massachusetts 01609
[2]Department of Natural Sciences, Assumption College, Worcester, Massachusetts 01609
[3]Department of Physics, Tufts University, Medford, Massachusetts 02155
Correspondence to: G. S. Iannacchione (E-mail: gsiannac@wpi.edu)

ABSTRACT: Modulated differential scanning calorimetry (MDSC) was used to measure the complex specific heat of the crystallization and melting transitions of nanocomposites of isotactic polypropylene (iPP) and carbon nanotubes (CNT) as function of CNT weight percent and temperature scan rate. In the last few years, great attention has been paid to the preparation of iPP/CNT nanocomposites due to their unique thermal and structural properties and potential applications. As the CNT content increases from 0 to 1 wt %, heterogeneous crystal nucleation scales with the CNT surface area. Above 1 wt %, nucleation appears to saturate with the crystallization temperature, reaching ~8 K above that of the neat polymer. Heating scans reveal a complex, two-step, melting process with a small specific heat peak, first observed ~8 K below a much larger peak for the neat iPP. For iPP/CNT samples, these two features rapidly shift to higher temperatures with increasing ϕ_w and then plateau at ~3 K above that in neat iPP for $\phi_w \geq 1$ wt %. Scan rates affect dramatically differently the neat iPP and its nanocomposites. Transition temperatures shift nonlinearly, while the total transition enthalpy diverges between cooling and heating cycles with decreasing scan rates. These results are interpreted as the CNTs acting as nucleation sites for iPP crystal formation, randomly pinning a crystal structure different than in the neat iPP and indicating complex transition dynamics. © 2013 Wiley Periodicals, Inc. J. Appl. Polym. Sci. 130: 587–594, 2013

KEYWORDS: Composites; phase behavior; self-assembly; thermal properties

Received 7 November 2012; accepted 19 February 2013; published online 20 March 2013
DOI: 10.1002/app.39204

INTRODUCTION

Since their discovery in 1991,[1] carbon nanotubes (CNTs) have emerged as a new class of nanosized particles for incorporation into various polymer systems, attracting considerable interest from basic science and industry. As a result of the exceptional intrinsic properties of CNTs, novel composite materials can be envisaged, that exhibit unique property enhancements, at CNT loadings much lower than in conventional composite technology.[2] In the field of thermoplastic nanocomposites, reported property enhancements include improved mechanical performance,[3,4] high thermal and electrical conductivity,[5–7] increased crystallization rate,[8–10] and altered rheological behavior.[11,12] However, a fundamental understanding of these nanocomposites is still lacking.

Because of its outstanding properties, low price, and wide applicability, isotactic polypropylene (iPP) is among the most well studied thermoplastics, with widespread application in various composite materials. Over the years, iPP has been reinforced with a wide range of fibers (e.g., carbon, glass, and natural fibers), essentially aiming at improving its mechanical performance. However, the emergence of CNTs as filler particles has paved the way for potential new applications, in fields, which so far have required the use of expensive custom synthesized polymers. For instance, a potentially important application is the use of nanocomposite films for the shielding of electromagnetic interference (EMI).[13,14] The requirements of a material for EMI shielding are manifold, as the film needs to be thin and transparent, yet mechanically stable and displaying a sufficiently high electrical conductivity. The use of CNTs as filler particles in iPP may provide a way to fulfill these requirements, as their incorporation simultaneously provides mechanical reinforcement as well as electrical conductivity. A prerequisite for the latter, however, is the achievement of an electrically conductive percolating network of nanofiller particles, at low enough loading to preserve the materials transparency.[14]

The phase transition behavior of iPP from the melt to the mesomorphic phase to the monoclinic crystal has been previously

studied by traditional DSC.[15] It has been long recognized that the addition of CNTs significantly affects the crystallization behavior and resulting crystalline morphology of the iPP matrix. However, high resolution complex calorimetry beyond traditional DSC has not been reported for nanocomposites. The CNTs were found to strongly nucleate iPP crystallization, resulting in a transcrystalline morphology.[16–18] This highly oriented columnar morphology, extending over the entire fiber-matrix interface, is significantly different from the spherulitic crystal growth commonly encountered in neat iPP. It is, however, generally not associated with polymorphism, unless when crystallized from the sheared melt around a pulled fiber.[19] The origin of transcrystallinity has been the subject of intensive research and is still a matter of debate. Its development is associated with the high density of heterogeneously nucleating sites on the fiber surface, restricting crystal growth to the direction perpendicular to the fiber, with the crystal c-axis aligned in the fiber long-axis.[20] However, several additional factors are believed to influence its formation, such as epitaxial crystal growth based on lattice matching, surface energy, and topology of the fiber, flow-induced crystallization, or residual stresses resulting from a mismatch in the thermal expansion coefficients of fiber and matrix.[16]

Transcrystallinity has also been encountered in a number of other polymer nanocomposite systems. For instance, nylon-6 crystals were reported to grow perpendicular to dispersed clay platelets,[21] whereas CNTs were found to template the growth of polyethylene crystals in a direction perpendicular to the nanotubes long-axis.[22,23] Crystallization from dilute solution was found to induce structures strongly resembling the "shish-kebab" morphology in polyethylene and nylon-6,6.[24] For iPP/CNT nanocomposites, finally, several reports suggested the occurrence of transcrystallinity, however without providing experimental evidence.[9,25–28] Moreover, contradictory findings subsist as to the possible occurrence of polymorphism in iPP nanocomposites containing CNTs.[26,29]

In this study, we report on the complex calorimetry of crystallization and melting behavior of neat iPP and well dispersed iPP/CNT nanocomposite thin films as a function of CNT content and temperature scan rate. For the iPP/CNT samples, CNT content varied from 0.01 to 5 weight percent (wt %) and the baseline temperature scan rate varied from $\pm$ 0.5 to 4 K min^{-1}. In all measurements, the crystallization and melting calorimetric signatures were almost entirely nonreversible (imaginary) with only a very small feature discernible in the reversible (real) specific heat component, indicating their strong first-order character. The crystallization and melting temperatures, T_C and T_M, increase as a function of CNTs concentration. The enthalpy of crystallization and melting of the iPP/CNT samples increases strongly with increasing CNT content, saturating for CNT concentrations above 1 wt %. These results provide strong evidence that the CNT surface provides crystal nucleation sites for a different crystal phase than in the neat iPP, which becomes more dominant as the CNTs content increases. We also present the effect of temperature scan rates on the thermal evolution of neat iPP and iPP/CNT nanocomposites revealing a nonlinear driving of the transition temperatures and enthalpies. During subsequent melting, recrystallization phenomena may occur depending on the applied heating rate, the kinetics of which will be discussed in terms of polymer chain segment mobility.

Following this introduction, Section "Material and Sample Preparation" presents a review of the material and sample fabrication/handling along with a brief description of the calorimetric methods. The calorimetric results are presented and discussed in Section "Results and Discussions." Finally, conclusions are made and future directions suggested in Section "Conclusions."

MATERIAL AND SAMPLE PREPARATION

iPP with a molecular weight of about 38 kg mol^{-1} was obtained from Scientific Polymer Products, catalog #130, in powder form and has a crystallization temperature of 395 K and a melting temperature of 433 K at a scan rate of $\pm$ 2.5 K min^{-1}.[30] Multiwalled CNTs with diameter 140 $\pm$ 30 nm and lengths 7 $\pm$ 2 μm were purchased from MER Corporation and were produced by catalytic chemical vapor deposition with a stated purity of >90%. For further purification of CNTs, 1 g of the CNTs was suspended in a mixture of concentrated sulfuric acid and nitric acid (3 : 1 vol. ratio). This solution was placed in a Misonix water bath sonicator for 24 h at 323 K. The resultant suspension was diluted with deionized water and filtered through a 400 nm pore membrane (PTFE) until the water passing through the filter had a pH between 6 and 7. The dispersions were subsequently filtered to the desired concentration. The resulting CNTs had a pH of between 3 and 3.5 and were stable although the surface of the CNTs suffers oxidative damage. Scanning electron microscopy analysis showed that the CNTs were shortened between 30 and 40% of their original length, as expected given this treatment.

Nanocomposites were prepared by sonicating CNTs in xylene at 323 K in a flask for 30 min. The iPP polymer was added to the xylene containing the CNTs to form the different weight percent concentrations of CNT in the nanocomposites for the study. The solution was then heated and stirred by placing the flask in an oil bath on a hot plate. Once the iPP was completely dissolved, the solution was mixed slowly into a nonsolvent (a polar compound such as alcohol) with about a 5 $\times$ volume dilution. The resulting precipitate was dried and then pressed into a film using a compression molding hot press at a temperature of 473 K and pressure of 20.6–41.4 MPa. The samples were then crystallized at 403 K for 30 min and cooled to room temperature for handling.

Crystallization and melting thermographs of the polymer and nanocomposites were investigated using a Model Q200 from TA Instruments, under constant dry nitrogen flow after instrument calibration. Small pieces cut from unsheared films (total mass of 8–10 mg) were encapsulated in standard aluminum pans, and heated quickly to the starting temperature of 470 K to equilibrate for about 30 min. An empty aluminum sample pan was used as the reference. Cooling and subsequent heating scans were performed between 300 and 470 K at a baseline scan rate $\pm$0.5 K min^{-1} with a modulation time period of 60 s and a modulation amplitude 0.5 K (effective modulation rate of 2π (0.5 K)/(1 min) = $\pm$1 K min^{-1}). Scan rate effects were probed

by maintaining the modulation parameters and varying the baseline scan rate from 0.5 to 4 K min^{-1}, again with cooling followed by heating scans. All cooling and heating cycles were repeated at least twice to ensure the reproducibility of the results presented in this work.

The total specific heat is given by $C_p = \sqrt{C_p'^2 + C_p^2}$, where C_p' is the real and C_p is the imaginary parts of specific heat. The excess specific heat was determined by choosing a linear baseline over the entire temperature scan range ($\Delta C_p = C_p - C_{\text{baseline}}$). The total transition enthalpy is simply the integration of the excess specific heat over a consistent temperature range, for example, $\Delta H = \int \Delta C_p dT$. The transition temperatures are taken as the peak temperature of any ΔC_p feature.

RESULTS AND DISCUSSIONS

Crystallization Behavior of iPP and iPP/CNT Nanocomposites

Figure 1 shows the total excess specific heat as a function of temperature for neat iPP and iPP/CNT samples with ϕ_w from 0.01 to 5 wt %. The crystallization temperature for neat iPP occurred at 400.08 K at the scan rate −0.5 K min^{-1} and 395.13 K at the scan rate −2 K min^{-1}, in good agreement with the literature value.[30] As the CNTs content increases, the ΔC_p peak remains as sharp as in neat iPP, only changing amplitude slightly. Further, T_C shifts upward by +4.6 K for the 0.01 wt % sample and continues to increase with increasing ϕ_w reaching +7.5 K at 5 wt % of CNT. See top panel of Figure 2. In addition to the large ΔC_p peak associated with crystallization, there appears a small ΔC_p feature for the neat iPP ~9 K lower in temperature. This feature is likely the conversion to crystal of boundary regions between initially formed crystal domains. See inset of Figure 1. With the addition of CNTs, this small ΔC_p peak generally decreases in size and shifts closer to the main ΔC_p peak as ϕ_w increases, reaching ~2.5 K below T_C for the 2 wt % sample before disappearing in the 5 wt % sample. These results are consistent with the CNTs promoting the crystal phase and minimizing the delayed conversion of domain boundary regions.

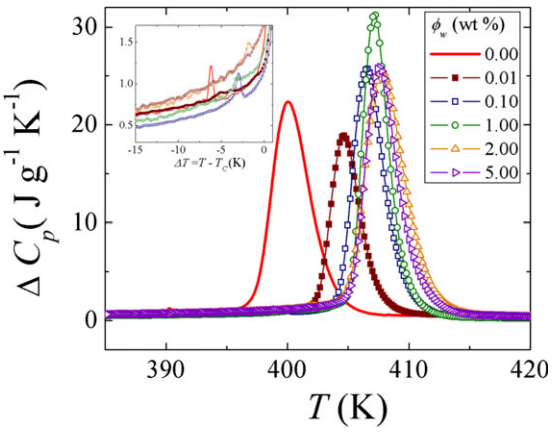

Figure 1. The total specific heat ΔC_p on cooling at −0.5 K min^{-1} through crystallization for neat iPP and iPP/CNT nanocomposites. See legend for wt % CNT. Inset shows an expanded view of the low temperature wings revealing a very small ΔC_p feature. See text for discussion. [Color figure can be viewed in the online issue, which is available at wileyonlinelibrary.com.]

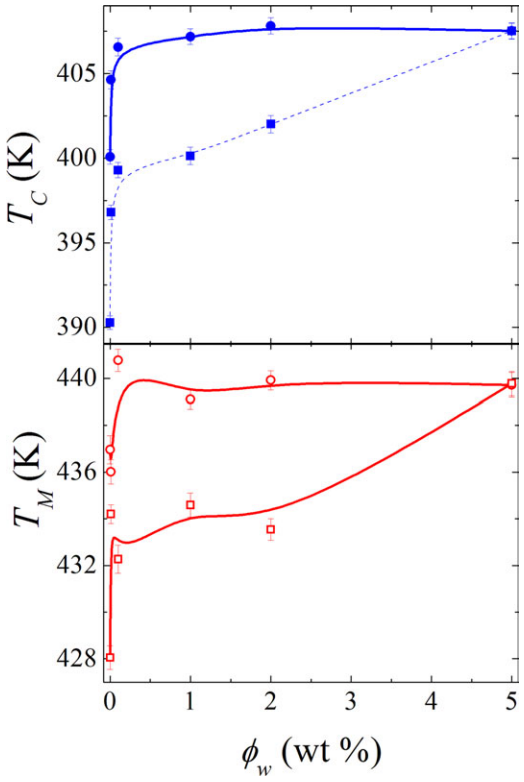

Figure 2. The crystallization and melting temperatures of the isotropic to mesomorphic α-monoclinic transition for neat iPP and iPP/CNT samples as a function of ϕ_w taken at ±−0.5 K min^{-1}. Top panel shows the large crystallization ΔC_p position (●) and the small secondary feature (■) on cooling. Bottom panel shows the temperature of two melting features, $T_{M,1}$ (□) and $T_{M,2}$ (○) on heating. Lines are guides to the eye. [Color figure can be viewed in the online issue, which is available at wileyonlinelibrary.com.]

The upper panel of Figure 2 shows the upward shift in the crystallization temperature T_C and that of the small ΔC_p feature that reaches a plateau value, evidently suggesting saturation of the nucleating effect. An upward shift in the crystallization onset and peak temperatures is observed, even for CNT loadings as low as 0.01 wt %, suggesting a high degree of crystal nucleation on the surface of the CNTs. The overall crystallization process is enhanced as a result of the presence of CNTs, providing a large number of nucleation sites. This results in an increase in T_C with respect to that of the homogeneously nucleated neat iPP. The crystallization behavior dependence on multiwall nanotube loading, as well as the plateau value of the crystallization onset, results from the increase in CNTs surface area as ϕ_w increases. The fact that the crystallization onsets level off at higher CNTs loadings and finally attain a plateau value is indicative of nucleation saturation. An incomplete CNT exfoliation at higher loadings provides a possible explanation, as poor CNTs dispersion at higher mass fractions implies that the outer surface of the nanotubes becomes increasingly inaccessible for crystal nucleation. Incomplete exfoliation of CNT bundles may be due to van der Waals interactions and nanotube clustering. Alternatively, from a certain loading onward, the crystallization rate may level off as a result of the fact that crystal growth becomes the rate-determining factor. Further increasing the

loading does effectively increase the nuclei density, but under the resulting time and temperature conditions crystallization proceeds more slowly, resulting in a leveling off of the crystallization onset. The rate-determining factors can either be the high crystallization temperature, resulting from the nucleating action, and diminishing the thermodynamic driving force for crystallization, or limitations in the diffusion of polymer chains toward the growing crystal front. The latter might result from reduced polymer mobility and from chain diffusion constraints in a geometrically confined space, as the average interparticle distance is reduced at higher loadings. With respect to the above discussion on the crystallization of the iPP matrix, it is worth noting that the nucleating action of CNTs, increasing the crystallization temperatures by 8 K, is comparable to that of conventional nucleating agents. Indeed, shifts of up to 15 K have been reported after incorporation of sodium benzoate into iPP.[31] Moreover, saturation of the nucleating effects was also observed for such conventionally nucleated systems[31,32] and was attributed to agglomeration of the nucleating particles due to over-dosage, limiting the number of effective nuclei. A summary of transition temperatures, enthalpies for crystallization and melting for all samples on heating and cooling are given in Table I.

Melting Behavior of iPP and iPP/CNT Nanocomposites

Figure 3 shows the total excess specific heat as a function of $\Delta T = T - T_{M,2}$ for neat iPP and iPP/CNT samples with ϕ_w from 0.01 to 5 wt %. For clarity, the ΔC_p traces are shifted upward successively by 2 J g^{-1} K^{-1} and shifted in temperature with respect to the final melting peak. The melting temperature occurred for our neat iPP is 436.96 K at +0.5 K min^{-1} and in good agreement with the literature value of 433 K at +2.5 K min^{-1}.[30] As shown in Figure 3, melting of neat iPP appears to proceed in a two-step process with a first order ΔC_p peak at a temperature $T_{M,1}$ appearing first followed by a large first order ΔC_p peak at $T_{M,2}$ on heating. The melting temperature $T_{M,2}$ shifts upward by 3.8 K from 0.01 to 0.1 wt % samples and remains same for higher loading of CNT content. See bottom panel of Figure 2 for the ϕ_w behavior of $T_{M,1}$ and $T_{M,2}$. Clearly, the presence of CNTs and the prior crystallization history have dramatic impact on the melting behavior of the polymer matrix. Whereas the neat polymer matrix unambiguously shows a double melting ΔC_p behavior, the shape of the melting ΔC_p progressively evolves toward single melting with increasing CNT concentration. Indeed, the lower melting peak $T_{M,1}$ progressively shifts to higher temperature upon increasing the CNTs loading, until it finally coincides with the higher melting peak $T_{M,2}$ at 5 wt % CNT loading.

Multiple melting features are generally assumed to result from polymorphism, from the successive melting of crystal populations with distinct degrees of perfection, or from the rapid succession of melting-crystallization-melting. The impact of CNTs on the polymorphic behavior of iPP has been extensively reported over the years. Some authors reported that CNTs can induce crystallization of iPP in the hexagonal polymorphic, instead of the more common monoclinic R-form.[26] Since both polymorphs display distinct melting temperatures, the observed changes in the shape of the melting transition in the presence of CNTs might potentially be the result of an altered balance between crystal forms co-existing in the sample.[32] This indicates that the CNTs surface not only nucleates the crystal phase but pins a particular crystal structures not common in neat iPP.

According to classical polymer crystallization theory, the melting temperature of a crystal T_M, is determined by its lamellar thickness.[33,34] The latter, however, is inversely proportional to the super cooling below the equilibrium melting point T^0_M. An equation relating the observed melting temperature to the crystallization temperature has been proposed, and the well-known linear Hoffman-Weeks method,[34] by which the equilibrium melting temperature is determined as the intersection of the experimentally recorded T_M plotted against T_C (with a slope slightly below 0.5 in most cases) and the line $T_M = T_C$ (slope = 1). This diagram is typically constructed for isothermally crystallized samples, but the strong nucleation in the presence of CNTs allows a similar diagram to be constructed for nonisothermally crystallized samples. Here, the lower melting peak temperature $T_{M,1}$ and higher melting peak temperature $T_{M,2}$ are plotted as a function of the corresponding crystallization peak temperature as shown Figure 4. The smaller ΔC_p peak at $T_{M,1}$ does very linearly with T_C with a slope of 0.51 and yields a T^0_M = 481.5 K, which is higher than the T^0_M commonly reported for neat iPP.[35] The larger ΔC_p peak at $T_{M,2}$ marking the final melting point has a larger slope of 1.47 and a T^0_M = 329.9 K. Clearly, on heating, the initial smaller ΔC_p peak behaves in a similar way as the melting in neat iPP and may represent regions far from CNT surface having a crystal structure similar to that in neat iPP. The final and larger ΔC_p peak behaves in a very different way with a T^0_M for below that in neat iPP indicating a crystal structure influenced by the CNT nucleation sites. Modulated differential scanning calorimetry (MDSC)

Table I. Summary of the Crystallization Temperature T_C, Total Crystallization Enthalpy δH_C, Melting Temperature $T_{M,2}$, and Total Melting Enthalpy ΔH_M for Neat iPP and iPP/CNT Nanocomposite Samples Using ±0.5 K min^{-1} and the Quasi-static MDSC Parameters, See Text

ϕ_w (wt %)	T_C (K)	$T_{M,2}$ (K)	ΔH_C (J g^{-1})	ΔH_M (J g^{-11})
0.00	400.08 ± 0.44	436.96 ± 0.61	92.33 ± 1.91	86.78 ± 2.21
0.01	404.64 ± 0.54	436.50 ± 0.52	74.47 ± 2.92	59.56 ± 3.22
0.10	406.57 ± 0.52	440.77 ± 0.48	93.53 ± 3.53	82.91 ± 3.51
1.00	407.19 ± 0.46	439.11 ± 0.42	102.97 ± 3.41	88.52 ± 3.62
2.00	407.82 ± 0.48	439.92 ± 0.41	122.74 ± 3.62	97.98 ± 3.41
5.00	407.52 ± 0.46	439.72 ± 0.53	118.36 ± 3.71	94.14 ± 3.80

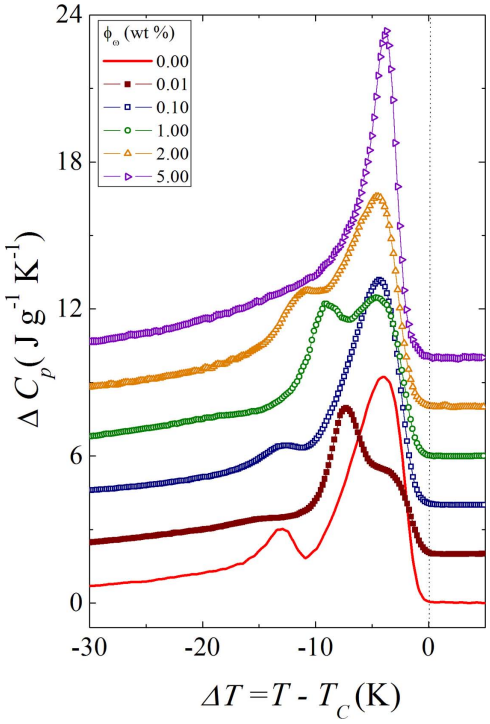

Figure 3. The total excess specific heat ΔC_p traces recorded during heating runs at +0.5 K min^{-1} through the melting region of the neat iPP and iPP/CNT nanocomposites containing loadings of CNTs listed in the legend. For clarity, the ΔC_p traces are shifted upward successively by 2 J g^{-1} K^{-1} with respect to the neat iPP trace. See legend for sample wt % CNT. [Color figure can be viewed in the online issue, which is available at wileyonlinelibrary.com.]

allows for a more detailed study of possible crystallization and melting phenomena. The real part of the specific heat is very small compared with the imaginary part for both crystallization and melting, both transitions being strongly first-order. On

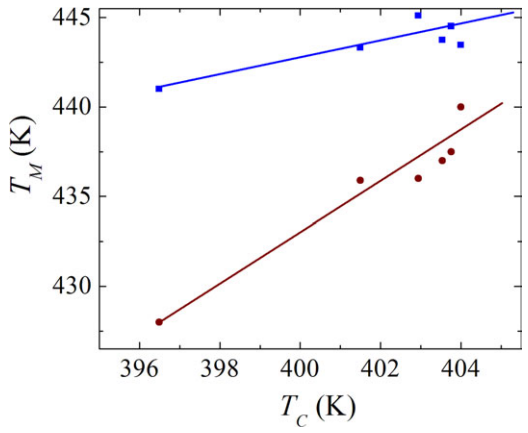

Figure 4. Melting temperatures $T_{M,1}$ (■) and $T_{M,2}$ (●) plotted against crystallization temperature for iPP filled with various loadings of CNTs. Crystallization and melting temperatures were obtained from nonisothermal MDSC experiments and straight lines from linear regression. See text for discussion. [Color figure can be viewed in the online issue, which is available at wileyonlinelibrary.com.]

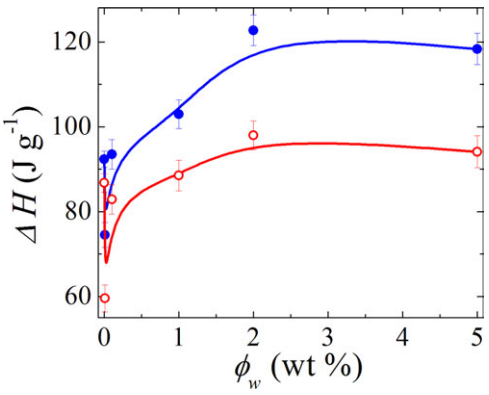

Figure 5. The total effective transition enthalpy of neat iPP and iPP/CNT nanocomposites on cooling (●) and heating (○) as a function of ϕ_w. Lines are guides to the eye. [Color figure can be viewed in the online issue, which is available at wileyonlinelibrary.com.]

melting, the total transition enthalpy decreases for $\phi_w = 0.01$ sample and then increases with increasing ϕ_w, saturating about 15 J g^{-1} above that for neat iPP at $\phi_w \geq 2$ wt % (see Figure 5). This indicates that the recrystallization phenomenon is progressively suppressed with increasing CNTs concentration. A summary of transition temperatures and enthalpies for all samples on heating and cooling are given in Table I.

Effect of Scan Rates on neat iPP and 2 wt % iPP/CNT

Since recrystallization essentially concerns the least perfect crystals present in the polymer, and requires time to occur, it is the sensitive to scan rate. The effect of increasing the cooling rate from −0.5 to −4 K min^{-1} on ΔC_p is shown in Figure 6. As the cooling rate increases for the neat the iPP (see top panel of Figure 6), the large ΔC_p peak shifts in temperature and eventually decreases in height and broadens in width for the fastest cooling rate of −4 K min^{-1}. As the heating rate increases from +0.5 to +4 K min^{-1}, see Figure 7, the ΔC_p traces do not shift in temperature but evolve in shape. The smaller ΔC_p peak at $T_{M,1}$ sharpens and increases in size while the larger ΔC_p peak at $T_{M,2}$ broadens and decreases in size.

The effect of increasing the cooling rate from −0.5 to −4 K min^{-1} on ΔC_p is shown in Figure 6. As the cooling rate increases for the 2 wt % iPP/CNT, see bottom panel of Figure 6, the large ΔC_p peak shifts in temperature and eventually decreases in height and broadens in width for the fastest cooling rate of −4 K min^{-1}. As the heating rate increases from +0.5 to +4 K min^{-1}, see bottom panel of Figure 7, the ΔC_p traces shift to lower temperature and also evolve in shape. The smaller ΔC_p peak at $T_{M,1}$ sharpens and increases in size while the larger ΔC_p peak at $T_{M,2}$ broadens and decreases in size.

The crystallization temperature (T_C) and the melting temperatures (T_M) as a function of scan rates are shown in Figure 8. The T_C on cooling decreases ~9 K for both neat iPP and 2 wt % iPP/CNT with increasing cooling rates from −0.5 to −4 K min^{-1}. The T_M upon heating decreases ~2 K for both neat iPP and 2 wt % iPP/CNT with increasing heating rates from +0.5 to +4 K min^{-1}. The T_C and T_M show linear behavior for neat iPP and nonlinear behavior for 2 wt % iPP/CNT. See in Figure 8.

Applied Polymer SCIENCE

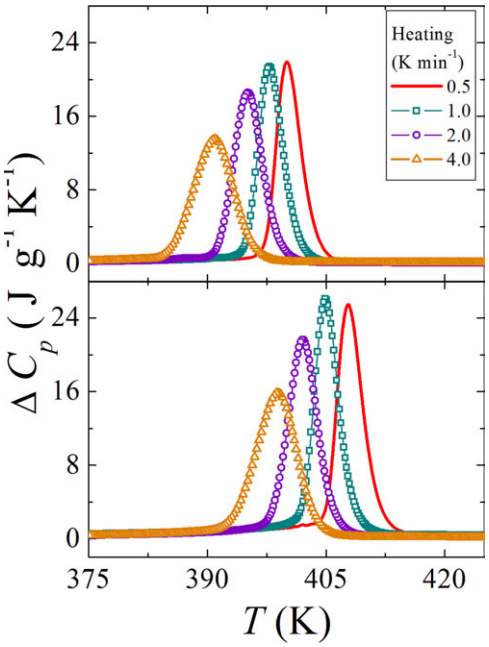

Figure 6. The total excess specific heat ΔCp on cooling from the isotropic to mesomorphic to α-monoclinic transitions as a function of continuous scan rate (K min^{-1}) for neat iPP (top) and 2 wt % of CNTs (bottom). For clarity, every 15th data point has been plotted. Quasi-static modulation parameters were used; 0.5 K temperature modulation amplitude and 60 s heating period, while the cooling rate was varied from -0.5 to -4 K min^{-1}. See legend. [Color figure can be viewed in the online issue, which is available at wileyonlinelibrary.com.]

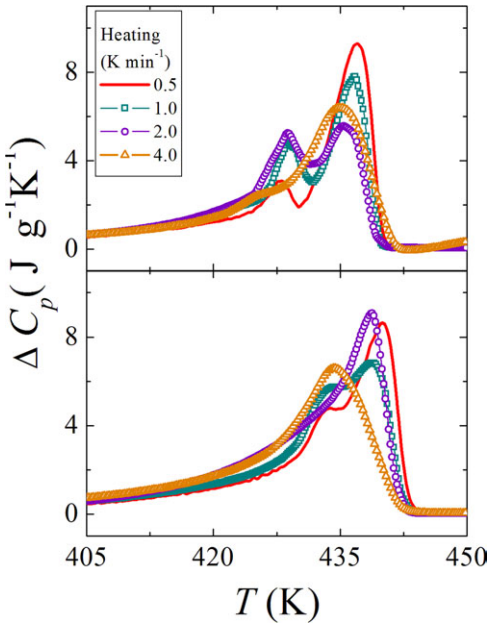

Figure 7. The total excess specific heat ΔCp on heating from the mesomorphic-α monoclinic to isotropic transitions as a function of continuous scan rate (K min^{-1}) for neat iPP (top) and 2 wt % of CNTs (bottom). For clarity, every 15th data point has been plotted. Quasi-static modulation parameters were used; 0.5 K temperature modulation amplitude and 60 s heating period, while the cooling rate was varied from -0.5 to -4 K min^{-1}. See legend. [Color figure can be viewed in the online issue, which is available at wileyonlinelibrary.com.]

Note that the extrapolated, zero scan rate, melting temperature is $T_M(0) = 437.81$ K and crystallization $T_C(0) = 401.25$ K, given by the dashed lines in Figure 8.

The effective transition enthalpy (ΔH) for both neat iPP and 2 wt % iPP/CNT as a function of scan rates is shown in Figure 9. The ΔH increases by 8 J g^{-1} on heating and is approximately constant as the function of cooling rate for neat iPP, whereas the ΔH is approximately constant on heating and decreases by 20 J g^{-1} as a function of cooling rate for 2 wt % iPP/CNT sample. The effective transition enthalpy diverges between cooling and heating cycles with decreasing scan rates. The enthalpy dependence for neat iPP and 2 wt % iPP/CNT samples reversed between cooling and heating. See in Figure 9.

For the neat iPP sample, recrystallization during fast heating is largely suppressed, as opposed to the situation under slow heating. In the presence of CNTs, recrystallization no longer seems to occur, resulting in a lower temperature of melting shown in Figure 7. Unlike under slow heating conditions, this result suggests that the final degree of crystal perfection remains lower in the nanocomposite sample than in the neat material, an effect even more accentuated for the rapidly cooled samples. Prominent double melting behavior is observed in the neat iPP sample, showing that the degree of crystal perfection after fast cooling is lower than in the slowly cooled sample. The nanocomposite sample, however, exhibits single melting behavior for higher scan rates, despite the much lower crystal perfection as compared to low scan rate, with only a slight shoulder attesting for recrystallization shown in Figure 7. Hence, the observed differences in the melting temperatures of the nanocomposite and neat iPP under fast heating conditions, convincingly show that recrystallization in both is reduced. The suppression of recrystallization is stronger in the nanocomposite than in the pure iPP film. This becomes particularly noticeable under kinetically unfavorable fast heating conditions, pointing at a reduced mobility of the polymer chain segments in the presence of CNTs.

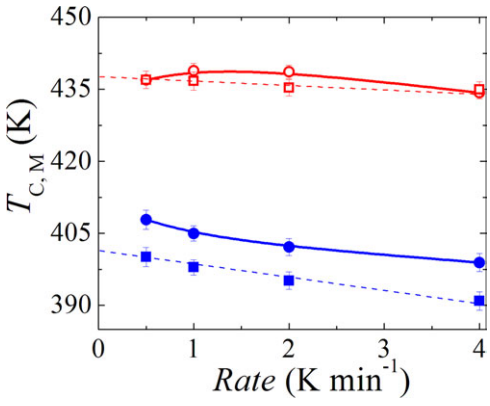

Figure 8. The main crystallization and melting transition temperatures as a function for neat iPP [cooling (■), heating (□)] and for 2 wt % iPP/CNT sample [cooling (●), heating (○)]. Lines are guides to the eye. [Color figure can be viewed in the online issue, which is available at wileyonlinelibrary.com.]

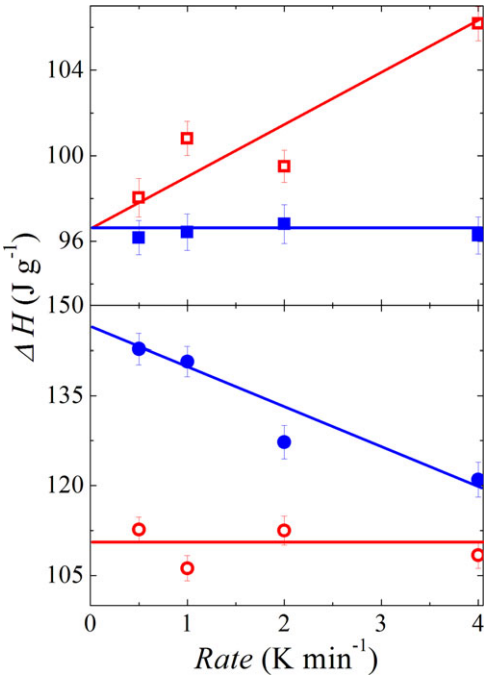

Figure 9. The total effective transition enthalpy as function of scan rate for neat iPP [top panel: cooling (■) and heating (□)] and for the 2 wt % iPP/CNT sample [bottom panel: cooling (●) and heating (○)]. Lines are guides to the eye. [Color figure can be viewed in the online issue, which is available at wileyonlinelibrary.com.]

However, when sufficient time is given to allow for crystal melting, reorganization, and subsequent recrystallization of existing crystal lamellae, the degree of crystal perfection can attain a level comparable with that in neat iPP. Potentially important factors capable of kinetically suppressing the recrystallization phenomena under the conditions chosen are the occurrence of polymer-CNT interactions, increases in viscosity, and effects related to geometrical confinement. Even though van der Waals interactions between iPP and CNTs are rather weak, they may affect the polymer crystallization since it is known to be extremely sensitive to subtle changes in the chain segment mobility. Therefore, even the weakest interactions might cause changes in the recrystallization behavior, especially in view of the tremendous interfacial area provided by the CNTs. Viscosity increases related to the formation of a percolating network of CNTs might equally affect the recrystallization behavior. Finally, geometrical confinement needs to be considered as the average distance between well dispersed CNTs becomes much smaller than the typical radius of gyration of the unperturbed polymer, hence also influencing its local segmental mobility and potentially hampering recrystallization phenomena. This was already noticed with respect to the nucleating action of the CNTs as well as in relation to their effect on the melting behavior of the matrix polymer. A key reason for their accentuated influence on the polymer in the considered nanocomposites is the much higher surface area they provide at equal mass fraction. Consequently, CNTs are also believed to more strongly affect the recrystallization behavior of iPP upon heating, as experimentally conformed at low heating rates shown in Figure 7. For higher heating rates, recrystallization is completely suppressed in the presence of CNTs, resulting in a lower melting temperature as compared to neat iPP.

In the CNT filled system, a slight shoulder at the low temperature end of the transition still accounts for some extent of recrystallization, but the crystalline perfection still does not reach that obtained in the neat material at the lowest rate. After the fastest cooling rates in this study, neat iPP shows clear double melting behavior for subsequent heating. Moreover, a slight shoulder at the low temperature end of the melting transition indicates that some of recrystallization even persists up to the highest heating rate. The recrystallization might be fully suppressed at even higher heating rates. For the first time, these observations therefore unambiguously evidence some degree of kinetic hindrance in CNT-filled iPP systems, because of alterations in the local mobility of the matrix polymer, induced by the surface of the CNTs. On the basis of the observation of an altered crystallization, melting, and recrystallization behavior, it is also anticipated that the presence of CNTs affects the local morphology of the polymer matrix, resulting in a very specific crystalline microstructure characteristic for the considered nanocomposite materials. A summary of transition temperatures, enthalpies on cooling and heating rates for neat and 2 wt % iPP/CNT samples are given in Table II.

CONCLUSIONS

The CNTs act as a strong nucleating agent for crystal growth. CNTs displayed nucleating effect comparable to that of

Table II. Summary of the Crystallization and Melting Temperatures, Total Effective Transition Enthalpies, and ΔC_p Peak Height (h_t) for Neat iPP (top) and 2 wt % iPP/CNT Sample (Bottom) as a Function of Baseline Temperature Scan Rates

ϕ_w (wt %)	±Rate (K min^{-1})	T_C (K)	T_M (K)	ΔH_C (J g^{-1})	ΔH_M (J g^{-1})	h_t (J g^{-1} K^{-1})
Neat (iPP)	0.5	400.08 ± 0.20	436.96 ± 1.89	96.16 ± 0.80	98.03 ± 0.90	21.91
	1.0	397.89 ± 1.60	436.70 ± 1.90	96.42 ± 0.85	100.81 ± 0.85	21.41
	2.0	395.13 ± 1.80	435.32 ± 1.70	96.80 ± 0.90	99.50 ± 0.75	18.56
	4.0	390.90 ± 1.90	434.94 ± 1.65	96.27 ± 0.87	106.20 ± 0.80	13.55
2 wt %	0.5	407.82 ± 0.21	436.96 ± 1.00	142.76 ± 2.60	112.66 ± 2.10	25.48
	1.0	404.97 ± 1.62	438.89 ± 1.50	140.67 ± 2.50	106.20 ± 2.12	26.07
	2.0	402.12 ± 1.80	438.66 ± 1.40	127.27 ± 2.80	112.50 ± 2.40	21.64
	4.0	398.90 ± 1.92	434.30 ± 1.30	121.00 ± 2.90	108.35 ± 2.20	15.89

traditional nucleating agents. An increase in the melting temperature after nonisothermal crystallization pointed at a higher degree of crystalline perfection in the presence of CNTs. The complex multiple melting behavior was interpreted in terms of recrystallization phenomena occurring during heating. A detailed MDSC study at varying cooling and heating rates revealed the partial suppression of crystal thickening as a result of reduced polymer mobility at fast cooling rates. In this article, a widely used commercial polymer is studied to gain wide applicability of the results. The CNTs used in this study are also commercially available, which means that they can be easily employed by the industry. The combination of these two important materials has many practical applications that require a deeper understanding of the thermo-physical properties and their connection to the microscopic order.

ACKNOWLEDGMENTS

This work was supported by the Department of Physics at WPI as well as grants from the NSF under the awards DMR-0821292 MRI, DMR-0602473, and DMR-1206010.

REFERENCES

1. Iijima, S. *Nature (London)* **1991**, *354*, 56.
2. Thostenson, E. T.; Ren, Z. F.; Chou, T. W. *Compos. Sci. Technol.* **2001**, *61*, 1899.
3. Coleman, J. N.; Khan, U.; Blau, W. J.; Gunko, Y. K. *Carbon* **2006**, *44*, 1624.
4. Coleman, J. N.; Khan, U.; Gunko, Y. K. *Adv. Matter* **2006**, *18*, 689.
5. Gojny, F. H.; Wichmann, M. H. G.; Fiedler, B.; Kinloch, I. A.; Bauhofer, W.; Windle, A. H.; Schulte, K. *Polymer* **2006**, *47*, 2036.
6. Qunaies, Z.; Park, C.; Wise, K. E.; Siochi, E. J.; Harrison, J. S. *Compos. Sci. Technol.* **2003**, *63*, 1637.
7. Haggenmueller, R.; Guthy, C.; Lukes, J. R.; Fischer, J. E.; Winey, K. I. *Macromolecules* **2007**, *40*, 2417.
8. Bhattacharyya, A. R.; Sreekumar, T. V.; Liu, T.; Kumar, S.; Ericson, L. M.; Hauge, R. H.; Smalley, R. E. *Polymer* **2003**, *44*, 2373.
9. Assouline, E.; Lustiger, A.; Barber, A. H.; Cooper, C. A.; Klein, E.; Wachtel, E.; Wagner, H. D. *J. Polym. Sci. Part B: Polym. Phys.* **2003**, *41*, 520.
10. Sandler, J. K. W.; Pegel, S.; Cadek, M.; Gojny, F. H.; Es, M. V.; Lohmar, J.; Blau, W. J.; Schulte, K.; Windle, A. H.; Shaffer, M. S. P. *Polymer* **2004**, *45*, 2001.
11. Potschke, P.; Fornes, T. D.; Paul, D. R. *Polymer* **2002**, *43*, 3247.
12. Kharchenko, S. B.; Douglas, J. F.; Obrzut, J.; Grulke, E. A.; Migler, K. B. *Nat. Matter* **2004**, *3*, 564.
13. Kim, H. M.; Kim, K.; Lee, C. Y.; Joo, J.; Cho, S. J.; Yoon, H. S.; Pejakovic, D. A.; Yoo, J. W.; Epstein, A. *J. Appl. Phys. Lett.* **2004**, *84*, 589.
14. Park, C.; Ounaies, Z.; Watson, K. A.; Crooks, R. E.; Smith, J.; Lowther, S. E.; Connell, J. W.; Siochi, E. J.; Harrison, J. S.; Clair, T. L. S. *Chem. Phys. Lett.* **2002**, *364*, 303.
15. Cao, J.; Sbarski, I. *Polymer* **2006**, *47*, 27.
16. Quan, H.; Li, Z. M.; Yang, M. B.; Huang, R. *Compos. Sci. Technol.* **2005**, *65*, 999.
17. Varga, J.; Karger-Kocsis, J. *Polymer* **1995**, *36*, 4877.
18. Wang, C.; Liu, C. R. *Polymer* **1999**, *40*, 289.
19. Bruckner, S.; Meille, S. V.; Petraccone, V.; Pirozzi, B. *Prog. Polym. Sci.* **1991**, *16*, 36.
20. Assouline, E.; Wachtel, E.; Grigull, S.; Lustiger, A.; Wagner, H. D.; Marom, G. *Polymer* **2001**, *42*, 6231.
21. Dasari, A.; Yu, Z. Z.; Mai, Y. W. *Macromolecules* **2007**, *40*, 123.
22. Haggenmueller, R.; Fischer, J.; Winey, K. I. *Macromolecules* **2006**, *39*, 2964.
23. Trujillo, M.; Arnal, M.; Muller, A. J.; Laredo, E.; Bredeau, S.; Bonduel, D.; Dubois, P. *Macromolecules* **2007**, *40*, 6268.
24. Li, C. Y.; Li, L. Y.; Cai, W. W.; Kodjie, S. L.; Tenneti, K. K. *Adv. Matter* **2005**, *17*, 1198.
25. Avila-Orta, C. A.; Medellin-Rodriguez, F. J.; Davila-Rodriguez, M. V.; Aguirre-Figueroa, Y. A.; Yoon, K.; Hsiao, B. S. *J. Appl. Polym. Sci.* **2007**, *106*, 2640.
26. Grady, B. P.; Pompeo, F.; Shambaugh, R. L.; Resasco, D. E. *J. Phys. Chem. B* **2002**, *106*, 5852.
27. Georgiev, G.; Cabrer, Y.; Wielgus, L.; Schoen, S.; Ivy, D.; Cebe, P. *MRS Proc.* **2011**, 1312.
28. Georgiev, G.; McIntyre, M. B.; Judith, R.; Gombos, E. A.; Cebe, P. *MRS Proc.* **2011**, 1308.
29. Leelapornpisit, W.; Ton-That, M. T.; Perrin-Sarazin, F.; Cole, K. C.; Denault, J.; Simard, B. *J. Polym. Sci. Part B: Polym. Phys.* **2005**, *43*, 2445.
30. Miltner, H. E.; Grossiord, N.; Lu, K.; Loos, J.; Koning, C. E.; Mele, B. V. *Macromolecules* **2008**, *41*, 5753.
31. Jang, G. S.; Cho, W. J.; Ha, C. S. *J. Polym. Sci.* **2001**, *39*, 10011016.
32. Varga, J. *J. Macromol. Sci.* **2002**, *41*, 1121.
33. Hoffman, J. D.; Davis, G. T.; Hannay, N. B. E. Jr. *Treat. Solid State Chem.* **1976**, *3*, 497.
34. Hoffman, J. D.; Weeks, J. J. *J. Res. Natl. Bur. Stand.* **1976**, *66A*, 13.
35. Miller, R. L. In Polymer Handbook, 4th ed.; Brandrup, J.; Immergut, E. H.; Grulke, A. Eds.; John Wiley & Son: New York, **1999**.